Journal of ELECTRONIC MATERIALS, Vol. 43, No. 4, 2014
DOI: 10.1007/s11664-014-2984-x

Sol–Gel Synthesis of Mn–Sn–Ti-Substituted Strontium Hexaferrite Nanoparticles: Structural, Magnetic, and Reflection-Loss Properties

MAJID JAMALIAN,[1,2] ALI GHASEMI,[1] and EBRAHIM PAIMOZD[1]

1.—Department of Materials Engineering, Malek Ashtar University of Technology, Shahin Shahr, Iran. 2.—e-mail: mjscience@yahoo.com

Substituted strontium hexaferrite nanoparticles with the chemical formula $SrFe_{12-x}(MnSn_{0.5}Ti_{0.5})_{x/2}O_{19}$($x$ = 0–2.5, in a step of 0.5) were prepared by a sol–gel method. Phase identities and crystal structure of the synthesized nanoparticles were investigated by x-ray diffraction. The morphology of the nanopowders was determined by field emission scanning electron microscopy. Results obtained from Fourier-transform infrared spectroscopy revealed the presence of stretching and bending modes in the citrate complex. Mössbauer spectroscopy (M_S) revealed occupancy of the hexagonal lattice structure by non-magnetic Mn^{2+} –Sn^{4+} –Ti^{4+} cations. Magnetic properties were measured by use of a vibrating sample magnetometer. The results showed that saturation magnetization and coercivity decreased with increasing x content. Microwave absorption properties were investigated by use of a vector network analyzer. It was found that the maximum reflection loss of substituted Sr-ferrite 1.6 mm thick reached −41.8 dB at a frequency of 4.3 GHz and a bandwidth of 7.5 GHz, with reflection loss being higher than −25 dB. These results imply that the prepared composites are good candidates for absorbers in the gigahertz frequency range.

Key words: Magnetic properties, microwave absorption, reflection loss, strontium ferrite

INTRODUCTION

Recently, electromagnetic interference (EMI) has been studied in depth because of the development of devices operating in the gigahertz range, for example satellites, cellular telephones, wireless instruments, radar, etc.[1–3] It is thus becoming increasingly difficult to ignore the effects of microwave energy, i.e. energy in the frequency range 300 MHz to 300 GHz (wavelengths between 1 mm and 1 m).[4] The rapid development of communication devices utilizing electromagnetic waves with gigahertz frequencies has caused serious trouble. Absorber materials which can prevent electromagnetic interference are available.[5–7] M-type hexaferrites are the most promising materials widely used for the development of microwave absorbers in the high gigahertz range because their large anisotropy field ($H_a \sim 17$ kOe) results in magnetic resonance in the range 2–52 GHz.[8] Nevertheless, resonance absorption in the high and low gigahertz range is weak because of the low magnetic permeability of ferrites.[9] The intrinsic magnetic properties of M-type ferrites can be enhanced by substitution with Sr or Fe or both.[5–7,10]

$SrFe_{12-x}(MnSn_{0.5}Ti_{0.5})_{x/2}O_{19}$($x$ = 0–2.5) was prepared by the conventional sol–gel method. This technique resulted in nanosized particles with a wide size distribution and chemical homogeneity. Numerous studies have attempted to explain the effect of substitution of Fe ions with a variety of metal cations in strontium (SrM) and barium (BaM) ferrites, to discover how to improve magnetic and microwave

(Received June 9, 2013; accepted January 2, 2014; published online January 24, 2014)

properties of, for instance, Mn–Co, Ti–Co,[11] Nd–Co,[12] Al–Cr,[9] Ni–Sn,[13] Er–Ni,[14] etc. In most research on *M*-type ferrites, reflection loss often occurred in the frequency range 8–18 GHz; in this study maximum reflection loss (RL) with broad bandwidth occurred at lower frequencies (2–10 GHz).

In 2012, Sharbati et al.[15] conducted a study on Mn–Ti–Sn-substituted strontium ferrite synthesized by the citrate sol–gel method in which maximum reflection loss (−39 dB) with a bandwidth of 1.9 GHz (RL > −20 dB) in the X band frequency range (8–12 GHz) was obtained. In contrast, in this paper we show that Mn–Sn–Ti substituted SrM can be an appropriate absorber with maximum RL of −41.8 dB, bandwidth of 7.5 GHz, and reflection loss higher than −25 dB in the frequency range 2.5–10 GHz.

Generally, the purpose of this study was to determine and explain the effects of Mn^{2+}–Sn^{4+}–Ti^{4+} co-doping substitution on electromagnetic wave absorption by an absorber in the gigahertz frequency range with a broad bandwidth.

EXPERIMENTAL PROCEDURE

In the sol–gel technique, first, a strontium citrate solution was formed from stoichiometric amounts of strontium chloride ($SrCl_2{\cdot}6H_2O$) and citric acid ($C_6H_8O_7$) in the molar ratio 1.5:1. This solution was then mixed with ferric chloride ($FeCl_3$) in proportions which furnished a set of compositions with an Fe/Sr ratio of 12. The resulting homogeneous solution of pH 0.5 was mixed with $TiCl_4$, $SnCl_4$, and $MnCl_2{\cdot}2H_2O$ to obtain the citrate complex of these precursors. The prepared samples were calcined at 900°C for 1 h in air. X-ray diffraction (XRD) analysis (Philips, MPD-X'PERT) of the doped Sr-ferrite was performed with Cu K_α radiation; patterns were recorded from 2θ (°) = 20 to 70. To investigate the microstructure and morphology of Sr-ferrite particles, field emission scanning electron microscopy (FESEM) (S-4160 Toshiba) analysis was conducted. Fourier-transform infrared spectroscopy (FTIR) (ISCO-680PLUS) was used for identification of functional groups and bond types. Mössbauer spectroscopy (Cryorac, Troisdorf, Germany) was used to determine the preferential occupancy of hexagonal structure sites by dopants. Magnetic properties of samples were evaluated by use of a vibrating sample magnetometer (VSM) (TM-XY-ZTB-SIH), up to a maximum applied field of 20 kOe. The microwave absorbers were prepared by mixing the doped SrM ferrite and poly(vinyl chloride) (PVC) in the mass ratio 70:30. The composites were pressed at a pressure of 5.5 MPa and fired at 220°C for 18 min. The thickness and diameter of prepared absorbers were 1.6 mm and 40 mm, respectively. Reflection loss of the absorbers was investigated by use of a vector network analyzer (VNA) (HP 8722ET).

RESULTS AND DISCUSSION

Evaluation of Structure and Morphology

Figure 1 shows the XRD patterns of $SrFe_{12-x}(MnSn_{0.5}Ti_{0.5})_{x/2}O_{19}$($x$ = 0–2.5) nanoparticles. The samples were almost single magnetoplumbite structure. Some studies have reported a redundant phase and a hexagonal SrM phase; in this work no secondary phases were observed in x-ray analysis.[12,14] The peaks of the doped strontium ferrite were not at the same precise positions as those of the undoped ferrite; intensities were also different. The shift in the position of the peaks was because of substitution of the Fe ions (0.64 Å) with Mn–Sn–Ti ions of different ionic radius. For $SrFe_{12-x}(MnSn_{0.5}Ti_{0.5})_{x/2}O_{19}$($x$ = 0–2.5), diffraction peaks at 2θ = 30.325°, 32.352°, 34.183°, and 40.378° arose from the (110), (107), (114), and (205) planes, respectively (JCPDS: 33-1340, 01-072-0739, 01-079-1412). Doping of the ferrite with Mn^{2+}, Sn^{4+}, and Ti^{4+} seemed to rearrange the hexagonal structure to furnish a single-hexagonal phase.[16] Different properties, e.g. cell constants (a, c, and c/a) and cell volume (V) were calculated by use of appropriate formulae:

$$\frac{1}{d} = \frac{4}{3}\left(\frac{h^2 + hk + k^2}{a^2}\right) + \frac{l^2}{c^2}, \quad (1)$$

$$V = 0.8666a^2 \quad (2)$$

where "d" is the distance between two crystallographic planes (hkl) and "a" is the unit cell parameter.

Table I shows the lattice parameters of these samples. Variable behavior is observed for lattice constants a and c of these samples. In general a gradually decreases with Mn–Sn–Ti concentration up to the stoichiometric amount x = 1 (5.691 Å) and

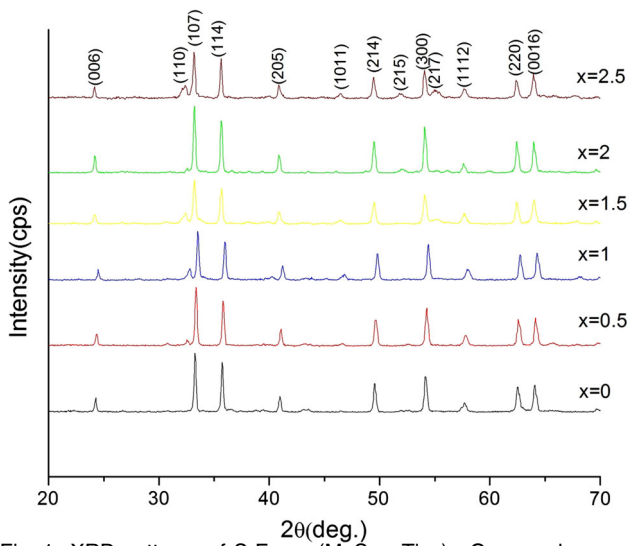

Fig. 1. XRD patterns of $SrFe_{12-x}(MnSn_{0.5}Ti_{0.5})_{x/2}O_{19}$ powders prepared with x content: (a) 0, (b) 0.5, (c) 1, (d) 1.5, (e) 2, (f) 2.5.

Table I. Lattice parameters of $SrFe_{12-x}(MnSn_{0.5}Ti_{0.5})_{x/2}O_{19}$ (x = 0, 0.5, 1, 1.5, 2, 2.5)

$SrFe_{12-x}(MnTi_{0.5}Sn_{0.5})_{x/2}O_{19}$	a (Å)	c (Å)	c/a	V (Å^3)
x = 0	5.728	21.160	3.694	601.6
x = 0.5	5.711	21.270	3.724	601.2
x = 1	5.691	21.143	3.715	593.4
x = 1.5	5.959	21.873	3.671	673.1
x = 2	5.998	18.895	3.150	589.1
x = 2.5	5.997	21.050	3.660	684.1

after an abrupt increase (5.959 Å) for x = 1.5 then becomes almost constant (5.900 Å) until x = 2.5. The reason for the decrease could be greater occupation of the Fe^{3+} sites by Mn^{2+} and Ti^{4+} with smaller ionic radii (0.46 and 0.61 Å, respectively) than Sn^{4+} (0.69 Å), giving rise to a shift in the peaks of XRD patterns toward larger angles (b and c x-ray patterns in Fig. 1). When the lattice constant increases, the reverse is probably happening, i.e. greater occupation of the Fe^{3+} sites by Sn^{4+} with larger ionic radii than Mn^{2+} and Ti^{4+} results in a tendency of the peaks to shift toward lower angles (d, e and f patterns).

Figure 2 shows FESEM microphotographs of $SrFe_{12-x}(MnSn_{0.5}Ti_{0.5})_{x/2}O_{19}$($x$ = 0–2.5) calcined at 900°C. The FESEM of the samples indicates the morphology and shape of the nanoparticles. It was found that the Mn–Sn–Ti additives significantly affected particle size and changed the morphology of $SrFe_{12-x}(MnSn_{0.5}Ti_{0.5})_{x/2}O_{19}$($x$ = 2, 2.5). Because it is possible for Mn–Sn–Ti additives to reduce the calcination temperature, the ferrite phase may be formed at lower temperatures and, thus, provide more growth time for nanoparticles up to 900°C. Moreover, nanoparticles with comparatively small sizes are prone to melt at a lower temperature; this is vigorously driven by their high surface energies owing to their large specific surface areas. Thus, more dopants result in a greater increase in particle size. EDS spectra of the samples are shown in Fig. 3, and the exact percentage of each element is listed in Table II. From Table II it can be deduced that as x increases the amounts of the elements gradually rise.

Figure 4 shows the FTIR spectra of $SrFe_{12-x}(MnSn_{0.5}Ti_{0.5})_{x/2}O_{19}$ (x = 0, 2.5) nanoparticles. Peaks at approximately 470 cm^{-1} and 550 cm^{-1} in the range between 400 cm^{-1} and 600 cm^{-1} are attributed to $SrFe_{12}O_{19}$.[17,18]

For a unit cell of M-type hexaferrite, there are five sublattices whose Fe^{3+} ions are substituted by metal cations. The interstitial sites of the close-packed layers contain three octahedral (2a, 12 k, 4f_2), one tetrahedral (4f_1), and one trigonal bi-pyramidal (2b) sites. The spin direction of 2a, 12 k, 2b sites is upward and for 4f_1, 4f_2 sites, it is downward. They were coupled by super-exchange interactions through the O^{2-} ions, forming the ferromagnetic structure.[19–22] According to Fig. 5, a good fit was achieved for substituted strontium ferrite using five sub-spectra corresponding to the 4f_1, 4f_2, 2a, 12 k, and 2b sites. The nonmagnetic dopants were placed on 12 k with upward spin direction causing reduction of the total magnetic moment. Further addition of dopants to the lattice resulted in a decrease in the total magnetization.[20]

Magnetic and Microwave Properties

Experimental hysteresis loops are compared in Fig. 6. Results obtained by use of the VSM are listed in Table III. It is clear the undoped sample had a larger coercive force (H_c), a larger hysteresis loop area, and a higher M_r than the other samples; the two later factors resulted in larger hysteresis loss. The coercivity of pure strontium ferrite was high (1259.3 Oe), because of strong uniaxial anisotropy along the c-axis of M-hexaferrite. On substitution with Mn, Sn, and Ti, coercivity was quickly reduced to 757.1 Oe at x = 1. There are two reasons for this behavior:

1 First, the main cause of the decrease in coercivity was the increase of mean particle size from 50 nm to 120 nm for the samples with x = 0 and x = 2.5, respectively.
2 According to Ghasemi and Morisako[23], the other reason could be reduction in the magnetocrystalline anisotropy field, because of the change of the easy axis of magnetization from the c-axis to the basal plane.

Further substitution with dopants further reduced coercivity, because of the decrease in in-plane anisotropy. The change in the magnetization is generally caused by rotation of spins or domain wall displacement.[23] Decreasing M_S can be explained by the occupation of lattice sites by Sn^{4+}, Ti^{4+} and Mn^{2+} ions. The nonmagnetic dopants were placed on 12 k with upward spin direction, causing reduction in the total magnetic moment. Accordingly, further addition of dopants to the lattice resulted in decreases of the first and second anisotropy constants, and concomitantly, a decrease in the anisotropy field (H_a).[23] It can be seen that magnetization of the MnSnTi-substituted samples (x = 0.5–2.5) was lower than that of the pure sample. Because the magnetic moment of Mn^{2+} (5μ_B) ions was equal to that of Fe^{3+} (5μ_B) ions, occupation of Fe^{3+} ion sites by Mn^{2+} ions had no effect on magnetic moment. Also, the presence of Ti^{4+} nonmagnetic ions at both spin-down and spin-up sites with the same probabilities compensated for their effect on each other. Therefore, occupation of the Fe^{3+} ion sites by Mn^{2+} and Ti^{4+} ions had no net effect on magnetic moment. But, because the ionic radii of Mn^{2+} (0.46 Å) and Ti^{4+} (0.61 Å) are different from that of Fe^{3+} (0.64 Å), a decrease in superexchange

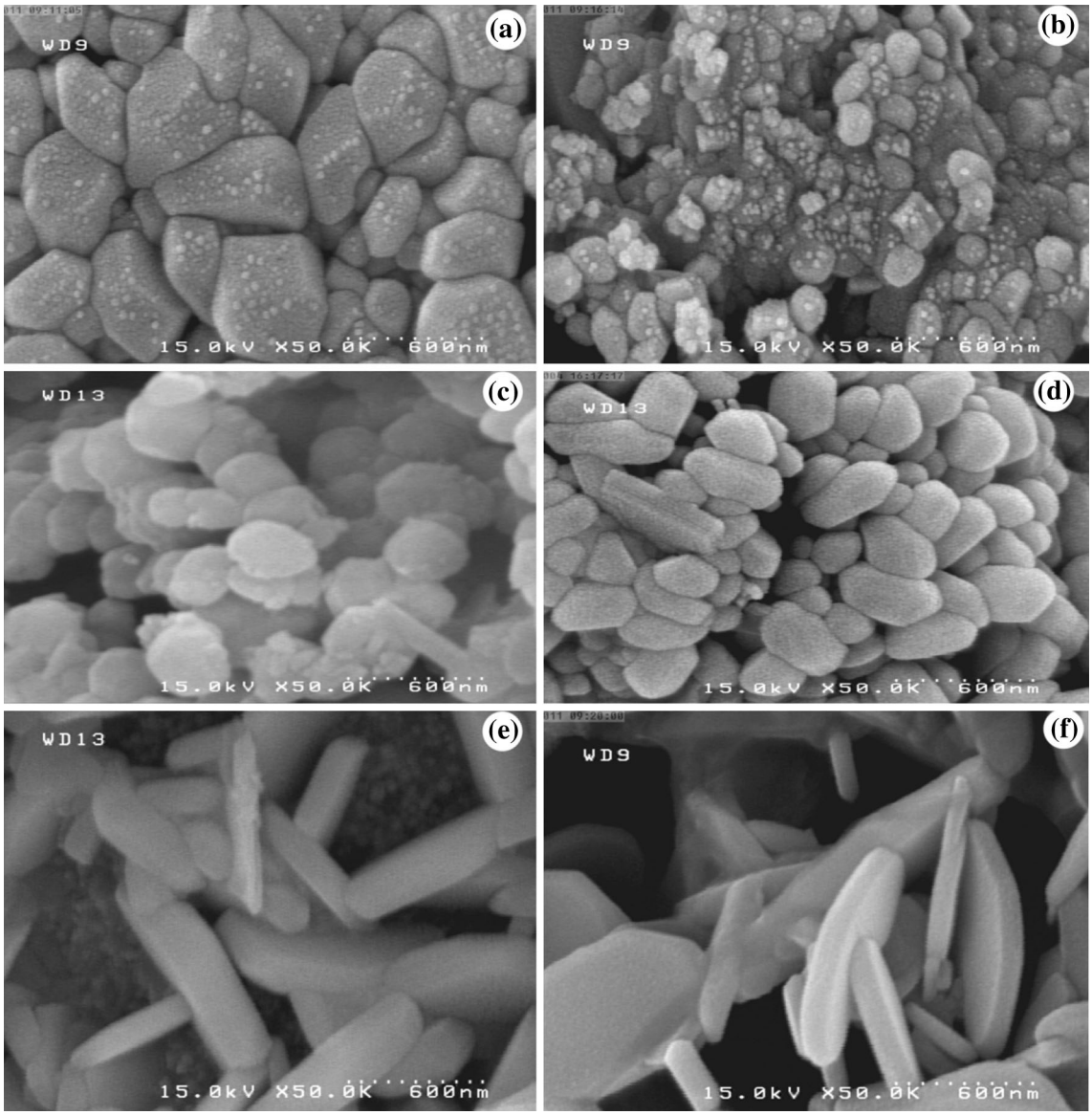

Fig. 2. FESEM micrographs of powders of $SrFe_{12-x}(MnSn_{0.5}Ti_{0.5})_{x/2}O_{19}$ with x content: (a) 0, (b) 0.5, (c) 1, (d) 1.5, (e) 2, (f) 2.5.

interactions between $4f_1$–$12\,k$ and $4f_1$–$2a$ was expected. Thus the magnetization of samples was reduced. As the amounts of nonmagnetic ions were increased, the superexchange interaction was further reduced, resulting in a decrease in the saturation magnetization.[20] The Sn^{4+} ion was nonmagnetic with its spins in the downward direction. This replaced iron ions at the octahedral ($12\,k$) sites. The net spin of the Fe^{3+} ions in the upward direction was thus reduced, thus reducing the total magnetic moment and the saturation magnetization.

For a metal-backed absorber reflection loss can be defined as a function of normalized input impedance. The normalized input impedance (Z_{in}) of a microwave-absorbing layer backed by a reflector is given by:

$$Z_{in} = \frac{Z_I}{Z_0} = \left(\frac{\mu_r}{\varepsilon_r}\right)^{0.5} \tanh\left[j2\pi(\mu_r\varepsilon_r)^{0.5} f d / c\right], \quad (3)$$

where Z_{in} is the normalized input impedance at the absorber surface, Z_I is the input impedance, Z_0 is the impedance of free space, μ_r and ε_r are the relative permeability and permittivity of the medium, f is the frequency of microwaves in free space, c is the velocity of electromagnetic waves, and d is the thickness of the absorber. Reflection loss, the ratio of reflected power to incident power, is related to Z_{in} as:

$$\text{Reflection loss (dB)} = 20\log_{10}\left[\frac{(Z_{in}-1)}{(Z_{in}+1)}\right]. \quad (4)$$

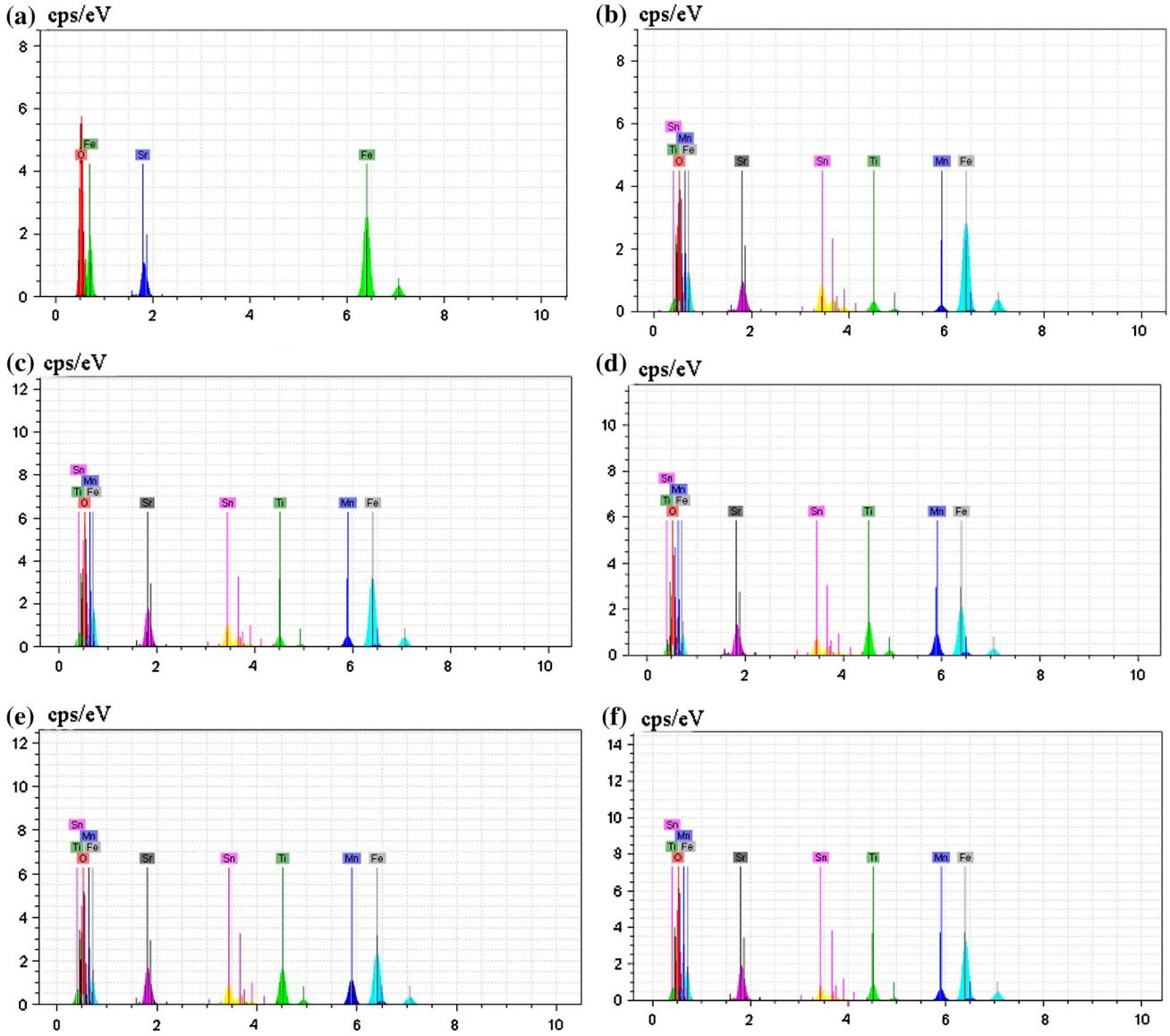

Fig. 3. EDS spectra of $SrFe_{12-x}(MnSn_{0.5}Ti_{0.5})_{x/2}O_{19}$ with x content: (a) 0, (b) 0.5, (c) 1, (d) 1.5, (e) 2, (f) 2.5.

Table II. Elemental compositions of $SrFe_{12-x}(MnSn_{0.5}Ti_{0.5})_{x/2}O_{19}$

x	Sr%	Fe%	Mn%	Sn%	Ti%	O%
0	8.91	59.05	–	–	–	32.04
0.5	7.42	57.31	3.12	8.57	3.67	19.91
1	10.34	50.36	5.65	8.15	4.41	21.07
1.5	9.92	48.76	7.56	9.22	8.33	23.95
2	8.95	45.89	11.06	9.36	9.28	17.45
2.5	9.65	39.10	13.57	9.75	11.08	19.85

Figure 7 shows the variation of reflection loss versus frequency in the range of 2.5–10 GHz for the x = 0–2.5 hexaferrite samples with 1.6 mm thickness and 70 mass% of ferrite. Here the bandwidth is defined as the frequency width in which the reflection loss is more than −25 dB. Measured microwave properties are listed in Table IV. From these data, we can see that an increase in x to 2.5 ($SrFe_{12-x}(MnSn_{0.5}Ti_{0.5})_{x/2}O_{19}$) resulted in the highest value of reflection loss (−41.8 dB) at the matching frequency of 4.3 GHz. In addition, both domain wall and natural resonance frequency were reduced. The ferromagnetic resonance f_r of strontium ferrite is given by the relationship:

$$2\pi f_r = \gamma\sqrt{H_\theta H_\varphi}, \tag{5}$$

where H_θ is the out of plane anisotropy field and H_φ is the in-plane anisotropy field. From this equation, it can be inferred that the ferromagnetic resonance frequency is closely related to the magnetocrystalline anisotropy fields H_θ and H_φ of strontium ferrites. In reality, H_θ and H_φ are related to Mn^{2+}, Sn^{4+}, and Ti^{4+} substitution.[23] Two resonance

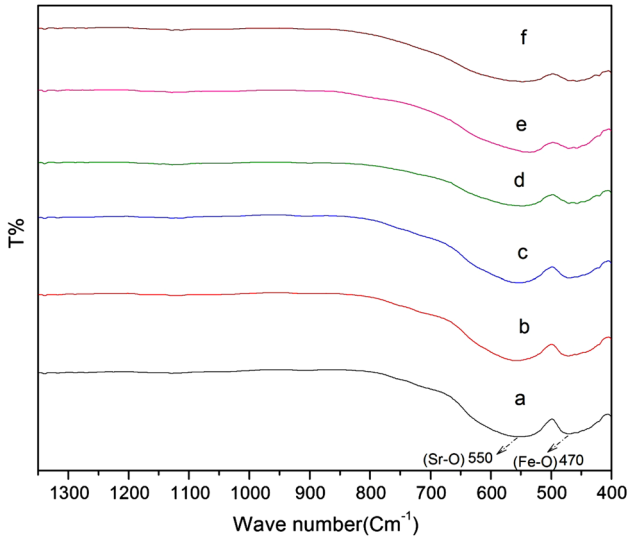

Fig. 4. FTIR spectra of $SrFe_{12-x}(MnSn_{0.5}Ti_{0.5})_{x/2}O_{19}$ with x content: (a) 0, (b) 0.5, (c) 1, (d) 1.5, (e) 2, (f) 2.5.

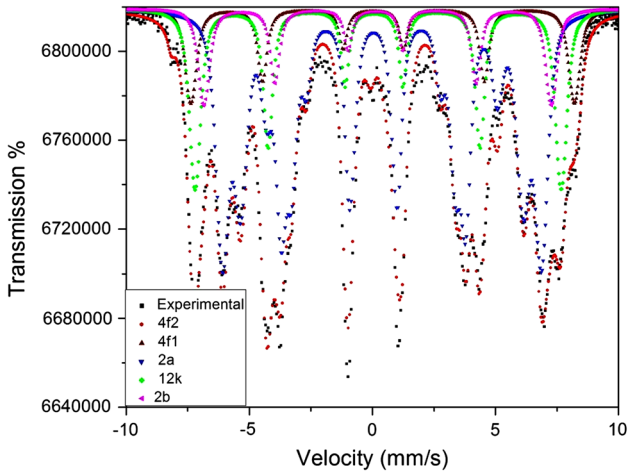

Fig. 5. Mössbauer spectra of $SrFe_{12-x}(MnSn_{0.5}Ti_{0.5})_{x/2}O_{19}$ (x = 2.5).

absorption peaks are detected for the ferrites. The resonance absorption peak at low frequency is related to domain wall resonance, and the peak at high frequency is related to natural resonance.[8,23] The most striking result to emerge from these data is that Mn–Sn–Ti substitution of strontium ferrite results in a wide bandwidth (> −25 dB) and high reflection loss in the frequency band 2.5–10 GHz. It is clear that the maximum bandwidth covered by this ferrite is approximately 7.5 GHz, with reflection loss being higher than −41.8 dB. Substitution of iron in ferrites by non-magnetic ions changes the direction of the magneto-crystalline anisotropy of the material from the c-axis toward the a–b basal plane, where the reason for this anisotropy is effective coupling of the spins of the magnetic ions and the crystalline electric fields which affects the ions via spin–orbit coupling.[20] Therefore, with such

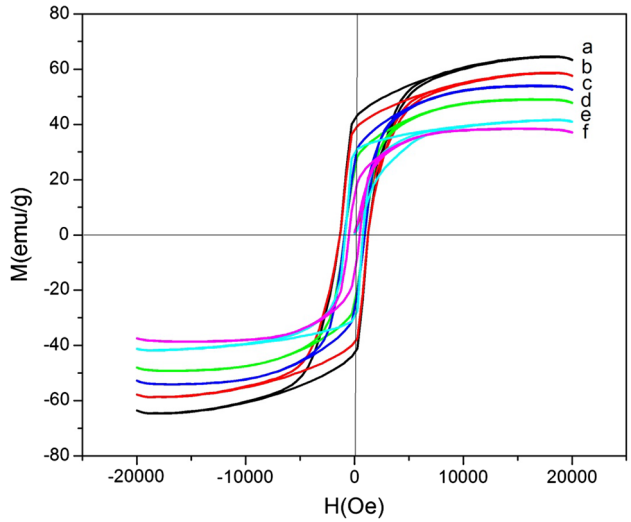

Fig. 6. Magnetic hysteresis loop of $SrFe_{12-x}(MnSn_{0.5}Ti_{0.5})_{x/2}O_{19}$ with x content: (a) 0, (b) 0.5, (c) 1, (d) 1.5, (e) 2, (f) 2.5.

Table III. The magnetic properties of different samples

$SrFe_{12-x}(MnTi_{0.5}Sn_{0.5})_{x/2}O_{19}$	M_S (emu/g)	M_r (emu/g)	H_c (Oe)
x = 0	64.2	43.2	1259.3
x = 0.5	58.6	39.3	1259.3
x = 1	54	31.1	757.1
x = 1.5	49.1	28.3	757.1
x = 2	41.7	31.0	751.7
x = 2.5	38.5	18.6	254.9

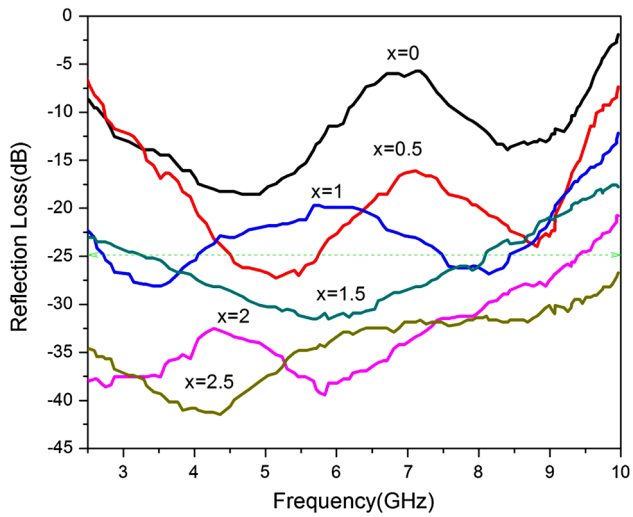

Fig. 7. Variation of reflection loss versus frequency for $SrFe_{12-x}(MnSn_{0.5}Ti_{0.5})_{x/2}O_{19}$ with: (a) x = 0, (b) x = 0.5, (c) x = 1, (d) x = 1.5, (e) x = 2, (f) x = 2.5.

Table IV. Microwave characteristics of $SrFe_{12-x}(MnSn_{0.5}Ti_{0.5})_{x/2}O_{19}$ (x = 0, 0.5, 1, 1.5, 2, 2.5)

$SrFe_{12-x}(MnTi_{0.5}Sn_{0.5})_{x/2}O_{19}$	Domain wall resonance (GHz)	Natural resonance (GHz)	Bandwidth (GHz) (RL > −25 dB)	Reflection loss (f_1) (dB)	Reflection loss (f_2) (dB)
x = 0	4.8	8.2	–	−18.8	−14
x = 0.5	4.2	8.1	1	−26.8	−24
x = 1	3.1	7.9	1.4	−28.1	−27
x = 1.5	2.5	5.8	1.7	−29	−31.6
x = 2	2.5	4.5	6.5	−38	−39.5
x = 2.5	2.5	4.3	7.5	−37	−41.8

substitution, the resonance frequency can be shifted to lower frequency.

CONCLUSIONS

A sol–gel method was used to synthesize Mn–Sn–Ti-substituted strontium ferrite nanoparticles. XRD results showed a single hexagonal phase for the substituted SrM ferrite. It was found that addition of the Mn–Sn–Ti significantly affected the grain size and morphology of $SrFe_{12-x}(MnSn_{0.5}Ti_{0.5})_{x/2}O_{19}$ (x = 2, 2.5). FTIR spectroscopy showed that functional groups, for example hydroxyl and carboxyl, were present on the surface of the nanoparticles. The saturation magnetization (from 64.2 emu/g to 38.5 emu/g) and coercivity (from 1259.3 Oe to 254.9 Oe) of the $SrFe_{12-x}(MnSn_{0.5}Ti_{0.5})_{x/2}O_{19}$($x$ = 0–2.5) were reduced by increasing x from 0 to 2.5 and the reflection loss of the nanocomposites was increased to −41.8 dB for the sample with x = 2.5.

REFERENCES

1. S.M. Abbas, A.K. Dixit, R. Chatterjee, and T.C. Goel, *J. Magn. Magn. Mater.* 309, 20 (2007).
2. J. Rong Liu, M. Itoh, and K. Machida, *J. Alloys Compd.* 389, 265 (2005).
3. S. Kimura, T. Kato, T. Hyodo, Y. Shimizu, and M. Egashira, *J. Magn. Magn. Mater.* 312, 181 (2007).
4. M. Oghbaei and O. Mirzaee, *J. Alloys Compd.* 494, 175 (2010).
5. A. Ghasemi, X. Liu, and A. Morisako, *J. Magn. Magn. Mater.* 316, e105 (2007).
6. J.F. Wang, C.B. Ponton, and I.R. Harris, *J. Alloys Compd.* 403, 104 (2005).
7. Q.Q. Fang, H.W. Bao, D.M. Fang, J.Z. Wang, and X.G. Li, *J. Magn. Magn. Mater.* 278, 122 (2004).
8. F. Tabatabaie, M.H. Fathi, A. Saatchi, and A. Ghasemi, *J. Alloy. Compd.* 470, 332 (2009).
9. M.N. Ashiq, M.J. Iqbal, and I.H. Gul, *J. Magn. Magn. Mater.* 323, 259 (2011).
10. W. Zhanyong, Z. Liuming, L. Jieli, Q. Huichun, Z. Yuli, F. Yongzheng, J. Minglin, and X. Jiayue, *J. Magn. Magn. Mater.* 322, 2782 (2010).
11. F. Tabatabaie, M.H. Fathi, A. Saatchi, and A. Ghasemi, *J. Alloy. Compd.* 474, 206 (2009).
12. C.A. Herme, P.G. Bercoff, and S.E. Jacobo, *Phys. B* 407, 3102 (2012).
13. P. Singh, V.K. Babbar, A. Razdan, S.L. Srivastava, V.K. Agrawal, and T.C. Goel, *J. Mater. Sci.* 41, 7190 (2006).
14. M.N. Ashiq, M.J. Iqbal, M. Najam-ul-Haq, P.H. Gomez, and A.M. Qureshi, *J. Magn. Magn. Mater.* 324, 15 (2012).
15. A. Sharbati, J.M.V. Khani, and G.R. Amiri, *Solid State Commun.* 152, 199 (2012).
16. Y.X. Gong, L. Zhen, J.T. Jiang, C.Y. Xu, and W.Z. Shao, *J. Magn. Magn. Mater.* 321, 3702 (2009).
17. W. Yongfei, L. Qiaoling, Z. Cunrui, and J. Hongxia, *J. Alloys Compd.* 467, 284 (2009).
18. X. Yang, Q. Li, J. Zhao, B. Li, and Y. Wang, *J. Alloys compd.* 457, 312 (2009).
19. V.G. Harris, A. Geiler, Y. Chen, S.D. Yoon, M. Wu, A. Yang, Z. Chen, P. He, P.V. Parimi, X. Zuo, C.E. Patton, M. Abe, O. Acher, and C. Vittoria, *J. Magn. Magn. Mater.* 321, 2035 (2009).
20. M. Mozaffari, A. Arab, M.H. Yousefi, and J. Amighian, *J. Magn. Magn. Mater.* 322, 2670 (2010).
21. Z.F. Zi, and Y.P. Sun, et al., *J. Magn. Magn. Mater.* 320, 2746 (2008).
22. J. Jalli, Y. Hong, S. Gee, S. Bae, J. Lee, J.C. Sur, G.S. Abo, A. Lyle, S. Lee, H. Lee, and T. Mewes, *J. IEEE Trans. Magn.* 44, 2978 (2008).
23. A. Ghasemi and A. Morisako, *J. Magn. Magn. Mater.* 320, 1167 (2008).